Research Article | Vol. 27, No. 7 | 1 Apr 2019 | OPTICS EXPRESS 9696
Optics EXPRESS

Fast information acquisition using spectra subtraction for Brillouin distributed fiber sensors

KUANGLU YU,[1,2] NAN GUO,[3] ZHIYUAN CAO,[1,2] SHUWEI LOU,[1,2] CHAO SHANG,[4,*] AND JING HE[5]

[1]*Institute of Information Science, Beijing Jiaotong University, Beijing 100044, China*
[2]*Beijing Key Laboratory of Advanced Information Science and Network Technology, Beijing 100044, China*
[3]*Department of Electronic and Information Engineering, The Hong Kong Polytechnic University, Kowloon, Hong Kong SAR*
[4]*Photonics Research Centre, Department of Electrical Engineering, The Hong Kong Polytechnic University, Kowloon, Hong Kong SAR*
[5]*Optoelectronics Research Centre, University of Southampton, Southampton, SO17 1BJ, United Kingdom*
**chao.shang@polyu.edu.hk*

Abstract: The traditional methods of extracting sensing information of a Brillouin distributed sensor is by curve fitting the Brillouin gain profiles along the fiber, we propose two concise and time-saving methods to process signals from only the frequency shifted section(s) of the fiber by subtracting the original spectrum from the sensing Brillouin spectrum. Experimental results validate that our methods can provide up to over 9 times faster information acquisition for a 10 km sensing fiber with 800 m frequency shifted section comparing with the traditional way. The proposed methods could be potentially attractive in getting information for the Brillouin distributed sensors as well as the Raman and Rayleigh distributed sensors especially when the processing speed is concerned.

1. Introduction

With distinguish advantages of high resolution, easy deployment, temperature and strain monitoring capability, Brillouin distributed fiber sensor is one of the main-stream scientific research topics of fiber optic sensors, and it has become commercially available in the last decade [1,2]. A great amount of research focuses on the front end technologies, *i.e.*, optical technologies, as coherent BOTDA [3], dynamic Brillouin [4], Differential Pulse Pair [5], pre-pulsed pump [6], sweep free BOTDA [7]. In the last couple of years, some work tackling the ever growing distributed sensing data were reported. Many common signal processing techniques are employed to denoise the spectra, including, wavelets denoising [8], non-local means denoising [9], adaptive linear prediction and cyclic coding [10], *et al*. In *Nature Communications*, Soto reported an image processing method to handle with the data, which claimed to have improved 100 fold sensor performance [11]. Some papers are aimed to process the spectra to obtain the sensing information efficiently as well, such as, continuous wavelet transform for phase optical time-domain reflectometer (Φ-OTDR) [12], two–dimensional edge detection method to improve Signal-to-Noise Ratio (SNR) and spatial resolution [13], iterative subdivision method to improve spatial resolution [14], online strain profile estimation method with two-stage adaptive algorithm [15], artificial neural network [16], principal component analysis based pattern recognition [17], as well as similarity comparison to obtain Brillouin frequency shift [18,19], *et al*.

A major obstacle to further reducing the processing time for the above-mentioned methods is that they all need to calculate full spectrum to acquire sensing information. In

#356569 https://doi.org/10.1364/OE.27.009696
Journal © 2019 Received 7 Jan 2019; revised 15 Feb 2019; accepted 19 Feb 2019; published 21 Mar 2019

Optics EXPRESS

practice, the Brillouin gain spectrum is normally obtained by Lorentzian curve fitting point by point and then the sensing information is retrieved from the central Brillouin frequency [20]. However, on the way to a higher solution, especially with 1 million points and beyond [21–24], to in-site real-time dynamic measurements [25–27], and to extra fine frequency resolution [28–30], the curve fitting process takes a very long time and it is neither target oriented nor effective, which makes those goals hard to achieve and some even unrealistic. Actually, not every single point along the fiber needs to be curve fitted, because a large range of the fiber's Brillouin frequency may only have jitters in a measurement, which is not necessary to be calculated, and only those points with frequency changes carries information and need be fitted and calculated.

In this manuscript, we propose two methods based on straight-forward spectrum subtraction which subtracts the measurement spectrum from the un-shifted spectrum before the spectrum is fitted. With this technique, a portion of the regular time with the traditional processing algorithm is needed to acquire Brillouin frequency shift information depending on the frequency shifted section length. Theoretical analysis on how to acquire Brillouin shift and to reduce the algorithm complexity is carried out before experimentally verification. This method could hopefully be adopted with the state-of-the-arts methods, such as, neural network, similarity method, as well as in other distributed sensing schemes, for example, Raman and Rayleigh sensors, helping them to retrieve distributed sensing information faster.

2. Spectra subtraction theory

In previous research, the sensing information, *i.e.*, the Brillouin gain peak along the fiber is obtained by curve fitting the gain profile point by point from one end to the other [3,5–7,9–11,14,15,20–24,26–30], and that profile ideally follows a Lorentzian shape as described below [31]

$$g_B(\nu) = g_0 \frac{(\Delta\nu_B/2)^2}{(\nu-\nu_B)^2 + (\Delta\nu_B/2)^2}, \tag{1}$$

where Brillouin spectrum linewidth, aka full-width at half-maximum (FWHM) $\Delta\nu_B$, original Brillouin frequency shift ν_B, and the peak gain g_0 are used to describe the Brillouin gain $g_B(\nu)$. To figure out the Brillouin frequency shifts (BFS) ν along the fiber, that is to find out differences between the original unshifted spectrum and, the strain and/or temperature changed spectrum, or often from the latter solely using itself as a frequency reference.

Since no frequency-shifted points can be tracked directly, the BFS is commonly obtained point by point along the fiber, including the points with no frequency shift. We propose to subtract the reference spectrum from the measurement one before fitting, and the differential action could help to distinguish the shifted and informative portion of spectrum from the unchanged. Then one could employ either the traditional fitting or calculate to obtain the BFS from the frequency shifted section(s) of the subtract spectrum, above two methods are named the Subtract and Fit Method (SFM) and the Subtract and Calculate Method (SCM), respectively. The two are both based on subtracted spectrum but uses different way to obtain the BFS, and them along with the traditional fitting algorithm are further discussed and compared with experimental data in later paragraphs.

A simulation is performed on a 10 km fiber whose central Brillouin frequency is 10.84 GHz. As an example, the fiber's 9-10 km section has 20 MHz frequency shift, and Gaussian white noise is added to the spectrum to simulate 25 dB SNR at the tail end. Those parameters are chosen to facilitate comparison with the experimental results. Due to the subtraction, a big portion depends on the measurement situation and the circumstance of the stimulated Brillouin spectrum (SBS) could be removed, and the remaining part, as shown in Fig. 1(c) which is the result of Fig. 1(b) minus Fig. 1(a), should theoretically be depicted in the form of

Optics EXPRESS

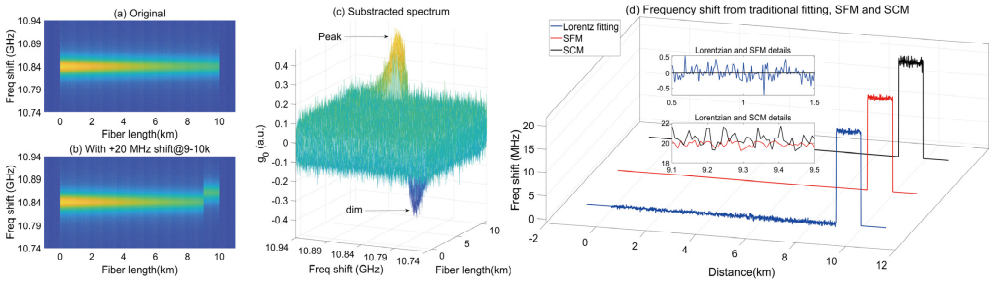

Fig. 1. (a) Original spectrum of 10 km fiber, (b) 9-10 km section at the far end with + 20 MHz shift, (c) subtracted spectrum, and (d), frequency shift from the traditional Lorentzian fitting (blue), the SFM (red) and the SCM (black). Insets: Details of the curves.

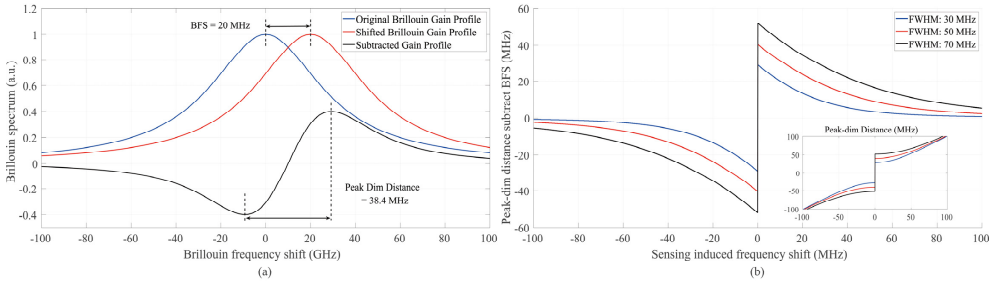

Fig. 2. Theoretical curves. (a) Demonstration of subtracting two Brillouin gain curves, (b) Frequency difference between peak-dim distance and sensing induced frequency shift, Δν. Insert: Peak dim distance relationship with the induced frequency shift.

$$\Delta g_B(\nu) = \frac{g_0(\Delta\nu_B/2)^2 \cdot [2\Delta\nu(\nu+\nu_B) - \Delta\nu^2]}{[(\nu-\nu_B-\Delta\nu)^2 + (\Delta\nu_B/2)^2] \cdot [(\nu-\nu_B)^2 + (\Delta\nu_B/2)^2]}, \tag{2}$$

where $\Delta\nu$ is the sensing induced frequency shift. Define $\Delta\nu_{PD}$ as the frequency difference of the peak and dim of the subtracted curve (See Fig. 2(a)) of a sensing point, the original and shifted gain profiles at that point are normalized and simulated as in blue and red respectively. $\Delta\nu_{PD}$ is determined by $\Delta\nu$ and the FWHM $\Delta\nu_B$ of the gain profile, and the relationship is depicted in Fig. 2(b) and in its inset. It shows that $\Delta\nu_{PD}$ is always larger than $\Delta\nu$, and this is especially significant when the shift is small. To find out $\Delta\nu$ with Eq. (2), one need to find out the peak and dim positions by differentiating Eq. (2) and then let the result to be zero as

$$0 = 3(\nu-\nu_B)^4 - 6\Delta\nu(\nu-\nu_B)^3 + (4\Delta\nu^2 - 2\gamma^2)(\nu-\nu_B)^2 - (2\Delta\nu\gamma^2 + \Delta\nu^3)(\nu-\nu_B) - \gamma^4. \tag{3}$$

Find the distance of the real roots of Eq. (3), which is $\Delta\nu_{PD}$. Then the Brillouin frequency shift $\Delta\nu$ can be further deduced as:

$$\Delta\nu = \pm\sqrt{-\Delta\nu_{PD}{}^2 - 4(\nu_B/2)^2 + 2\sqrt{\Delta\nu_{PD}{}^4 + 4\Delta\nu_{PD}{}^2 \cdot (\Delta\nu_B/2)^2}}. \tag{4}$$

$\Delta\nu_B$ is previously known and $\Delta\nu_{PD}$ is available from the subtracted spectrum. Then in the SCM, $\Delta\nu$ can be figured out with the above equation, and the complexity of the algorithm is reduced to minimum as no fitting is needed. However, it could be inaccurate for a noisy spectrum, thus discrete Meyer wavelet de-noising is employed in our algorithm. The simulation results of the SCM are illustrated in Fig. 1(d), $\Delta\nu$ by the Lorentz fitting is in blue while the subtraction method calculated frequency shift is in black. The insets show that the Lorentz method fits every point but actually gets noise for those un-shifted points, nevertheless, the SCM provides cleaner un-shifted region but slightly more noisy in the sensing area.

Optics EXPRESS

The SFM uses a more straightforward way, which is to use the subtracted spectrum as a criterion to obtain shifted points indices and carry out Lorentzian fitting on the frequency shifted points of the sensing spectrum as in the traditional way. This method comprises between processing speed and sensitivity, and the simulated SFM deducted Brillouin central frequency is drawn in red in Fig. 1(d).

2.1 Threshold for the subtraction algorithms

For both the SFM and the SCM, the points with value not equal to zero should be fitted if this is an ideal case without noise. However, in order to pick out the points with BFS from a noisy background, a proper threshold T is needed to distinguish subtracted gain from noise. Following the noise definition in [17,19,32], the variance along the fiber is calculated. In this manuscript, the noise is assumed to be similar along the fiber, and for convenience, T is defined as four times (i.e. SNR = 6 dB) the noise variance of the pre-fiber section of the spectrum.

2.2 Complexity of the algorithm

The traditional curve fitting method has a computational complexity on the order of $O(r_1N^2)$ for a spectrum with N points along the fiber [33], while the complexity of the SCM for the same object is on the order of $O(N)$, and the complexity of calculating part of the spectrum as done in the SFM is $O(r_2N^2/r_3)$, where the r_1 and r_2 is the number of iterations of the method, r_3 is the portion factor, which is the ratio of the whole fiber length over the shifted section(s) length.

The complexities of these algorithms for different numbers of resolved spatial points are theoretically calculated and illustrated in Fig. 3(a) in terms of processing time for a 10 km fiber with 9-10 km of it under 20 MHz strain. To fit all the curves in one figure, the Lorentzian fitting time curve is divided by a factor of 5. The same fitting algorithm is used in both the SFM and traditional methods to keep the results comparable. As shown by Ratio 1 in Fig. 3(a) that the SFM algorithm is about 10 times faster than that of the traditional way, while the SCM is even 3 times more effective than the former. With smaller numbers of spatial points processed, Ratio 1 go down due to the overhead calculations, but Ratio 2 stays relatively unchanged due to the fact that wavelet filtering consumes most of the time.

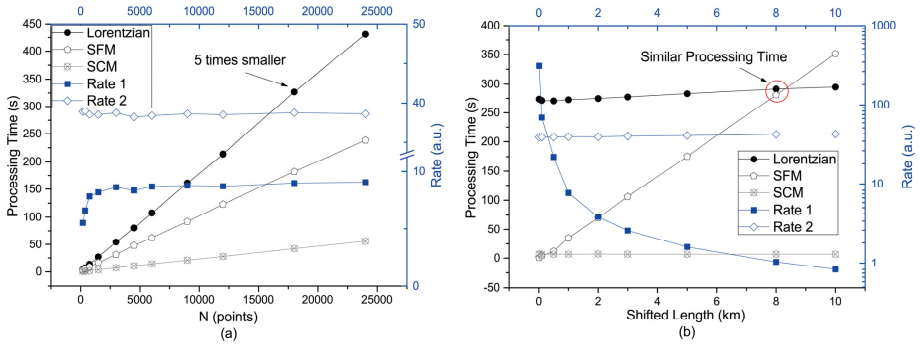

Fig. 3. Time consumption for the SCM, SFM, and traditional methods for (a), different spatial points number N, (b), different length of fiber with sensing induced frequency shift, Δv.

Simulation of a 10 km fiber (N was set to 3000) with different lengths having a 20 MHz SBS shift is shown Fig. 3(b), the processing time and complexity of the SFM go up linearly with increasing frequency shifted fiber length, which is proportional to the fitted point number N. We find out that when the frequency-shifted fiber length is 8 km, that is about 80% of the whole length in this case, the processing time is similar for the SFM and traditional fitting method. Furthermore, SFM consumes 18.9% more time for a fully shifted fiber due to the fitting decision mechanism. Therefore, it is less effective to use the SFM if

Optics EXPRESS

there is a large portion of shifted points along the sensing fiber. As expected, the simulated processing time of the SCM is always expected to be shorter than the traditional method.

3. Experiments with a BOTDA system

To verify the feasibility of our proposed SFM and SCM algorithms, an experimental BOTDA system was set up (Fig. 4) by removing the coding mechanism from the one used in [20]. A 10 km long single-mode fiber (SMF-28e + form Corning Inc.) with Brillouin frequency centered at 10.84 GHz was employed, the last 800 m of the fiber was placed in an oven which was set to be 30, 40, and 50 degree Celsius in turn, while the rest fiber was in room temperature, i.e., 25℃. The duration of the probe pulse was modulated to 20 ns (2 m spatial resolution) in the experiments, and the reflected signal was averaged for 1000 times before collected by a Tektronix real-time oscilloscope.

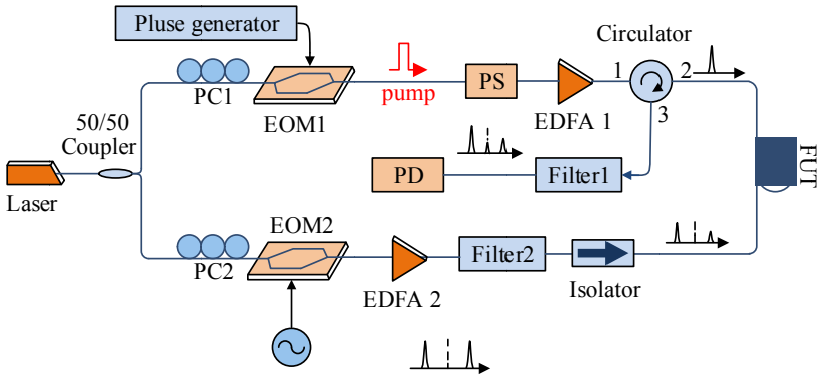

Fig. 4. B-OTDA experimental configuration. PC: polarization controller, EOM: electro-optic modulator, RF: radio frequency, PS: polarization scrambler, EDFA: Erbium doped fiber amplifier, FUT: fiber under test, PD: photodetector.

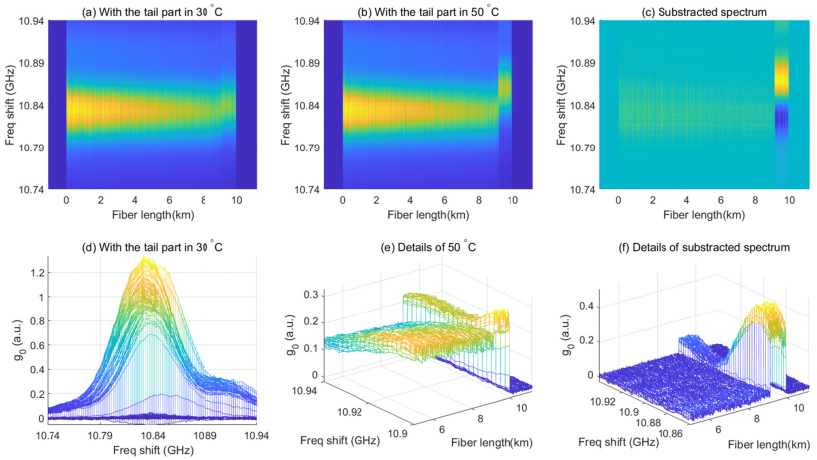

Fig. 5. Brillouin spectra obtain with our system with 1000 time averages with the tail parts in (a) 30 degree Celsius and (b) 50 Celsius, (c) is the subtraction of the former two, (d) is the xz view of (a), (e) and (f) are details of (b) and (c) respectively.

For example, the experimental data of 30 and 50℃ were used as reference and measurement spectrum, which were treated by our algorithm program to recover the BFS. Their Brillouin spectra and subtracted spectrum are shown in the upper row of Fig. 5, and the SNR of the reference and measurement spectra are calculated to be 26.76 and 27.37 dB

Optics EXPRESS

respectively. Detailed figures, Figs. 5(c)-5(e), show the fiber used has a second Brillouin peak at ~10.9 GHz, and a small disruption of optical power and central frequency caused by ambient temperature change, all of them consequently brought in deviations in the results.

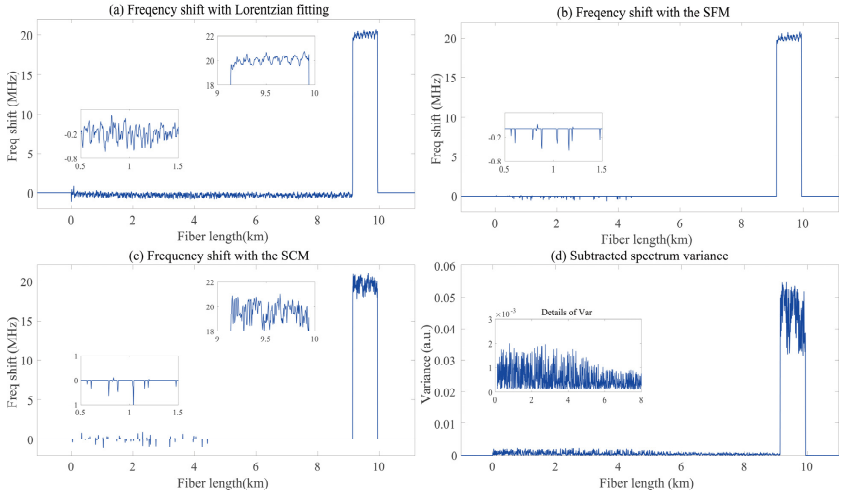

Fig. 6. Frequency shift with (a) the traditional Lorentzian fitting, (b) the SFM, and (c) the SCM for 20℃ temperature change, (d) is variance of the subtracted spectrum. The insets are details.

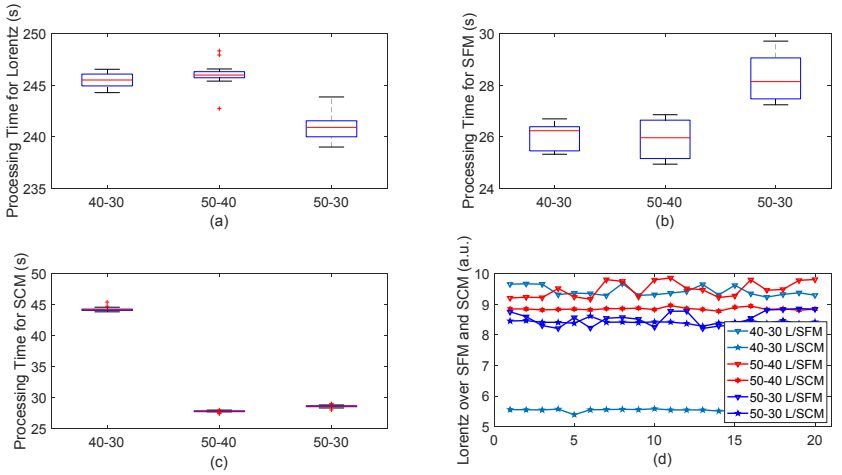

Fig. 7. Time costs for the Lorentz fitting, the SFM and the SCM.

The three methods were utilized to find out the BFS of the experimental data, and their results are illustrated respectively in Fig. 6(a)-6(c), the insets in those figures show that both the SFM and SCM results is less noisy than the traditional one in the unshifted section while the output of the SCM is more noisy than the other two in the shifted section. Figure 6(d) shows the variance of the data. Since the SFM and the SCM use a threshold to determine the fitting, they have much higher efficiency and largely reduce the amount of the points to be processed by finding out the frequency shifted section(s). The SFM keeps the same frequency shifted section details and accuracy comparing with the traditional way. However, not as expected, the original SCM doesn't work well with the presence of noises as it would be difficult to accurately obtain the peak and dim position. Therefore, it needs to be filtered and then fitted to find out the peak and dim values of the subtracted curve, which greatly slows it

down and its accuracy is also influenced by the filtering. The error also comes from the fiber's peak at ~10.92 MHz (as demonstrated in Figs. 5(d) and 5(e)), which caused an unwanted peak in the subtracted curve in Fig. 5(f), resulting in deviations from the subtraction curve in our model.

Then the processing time, as well as the accuracy of the methods were evaluated. Three data sets (40 - 30, 50 - 40, 50 – 30 averaged for 1000 times, corresponding to Time 1, Time 2 and Time 3 in Table 1) were calculated for 20 times each to find out an average processing time and accuracy for the three methods. Figure 7(a)-7(c) shows a boxplot of the processing time, and Fig. 7(d) depicts the time ratios of the three. Table 1 illustrates the time consumption and accuracy figures. The total average time reduction for the SFM is 89.04% with no accuracy lose, while it is 86.25% for the SCM with 0.26% accuracy drop.

Table 1. Time and Accuracy Compare for the Three Methods

Item / Method	Avg Time 1 (s)	Avg Time 2 (s)	Avg Time 3 (s)	Total Avg Time(s)	Time Reduction (a.u.)	Accuracy Reduction (a.u.)
Lorentz Fit (Traditional)	245.49	246.02	240.99	244.17	NA	NA
SFM	26.06	25.94	28.25	26.75	89.04%	NA
SCM	44.27	27.8	28.63	33.57	86.25%	–0.26%

4. Discussion

The SFM we proposed can obtain the Brillouin frequency shift from the spectrum saves 89% of the processing time than the frequently used Lorentzian fitting method with the same accuracy, thanks to the idea of locating the frequency shifted sections. While the SCM can be used to get the results in a fast way but not as fast as expected in theory, it is because of filtering and fitting needed to fight the noises and the unwanted sub-peak of the fiber. Comparing with the traditional way, our proposed methods are more vulnerable to noise, attributed to the lower signal power after deducting the common signal and the deteriorated SNR comparing with original signal. Therefore, in an extremely low SNR case, the traditional way is more preferable to retrieve the BFS. However, for a distributed sensor with a reasonable SNR, or if the induced frequency shift is significant, our proposed methods could save a large portion of the processing time, because instead of using all data fitting, the Brillouin peak shifted parts could be identified with a fitting threshold before being processed.

5. Conclusion

We have provided a fast subtraction technique to calculate the BFS of the fiber. Rather than fitting all the points along the fiber in the existing methods, only those frequency shifted points are fitted or calculated in the SFM and the SCM methods we proposed. In theoretical section, we obtained the relationship of the subtracted peak-dim distance and the actual Brillouin frequency shift, then discussed the algorithm complexity. The proposed methods are then verified by experimental data, which have shown that the SFM is about ten times faster than using the curve fitting way to process the Brillouin spectrum with the same accuracy, while the SCM is over 7 times faster with a small accuracy drop on average. The proposed methods could be easily combined with the front end techniques and they can be further applied to the Raman and Rayleigh sensors as well.

Funding

Beijing Jiaotong University Fundamental Research Fund Grant No. 2018JBM018; National Natural Science Foundation of China Grant No. 61805008, No. 61435006.

Optics EXPRESS

Acknowledgments

KY acknowledges the financial support from China Scholarship Council for funding him to visit Optoelectronic Research Centre, University of Southampton, and also his cooperate supervisor, Dr. Tracy Melvin. The authors would like to thank, Assoc. Prof. Hao Liang, Prof. Linghao Cheng in Jinan University, Guang Zhou, China for useful discussions, and also Assoc. Prof. Yanyan Zhu for revising the manuscript's language.

References

1. X. Bao and L. Chen, "Recent progress in distributed fiber optic sensors," Sensors (Basel) **12**(7), 8601–8639 (2012).
2. A. Motil, A. Bergman, and M. Tur, "[INVITED] State of the art of Brillouin fiber-optic distributed sensing," Opt. Laser Technol. **78**, 81–103 (2016).
3. L. Wang, N. Guo, C. Jin, K. Zhong, X. Zhou, J. Yuan, Z. Kang, B. Zhou, C. Yu, H.-Y. Tam, and C. Lu, "Coherent BOTDA Using Phase- and Polarization-Diversity Heterodyne Detection and Embedded Digital Signal Processing," IEEE Sens. J. **17**(12), 3728–3734 (2017).
4. M. Santagiustina and L. Ursini, "Dynamic Brillouin gratings permanently sustained by chaotic lasers," Opt. Lett. **37**(5), 893–895 (2012).
5. W. Li, X. Bao, Y. Li, and L. Chen, "Differential pulse-width pair BOTDA for high spatial resolution sensing," Opt. Express **16**(26), 21616–21625 (2008).
6. K. Kishida and C. H. Li, "Pulse pre-pump-BOTDA technology for new generation of distributed strain measuring system," in Proceedings of Structural Health Monitoring and Intelligent Infrastructure, L. Ou and Duan, ed. (Taylor & Francis Group, 2006), pp. 471–477.
7. A. Voskoboinik, O. F. Yilmaz, A. W. Willner, and M. Tur, "Sweep-free distributed Brillouin time-domain analyzer (SF-BOTDA)," Opt. Express **19**(26), B842–B847 (2011).
8. M. Amiri Farahani, M. T. V. Wylie, E. Castillo-Guerra, and B. G. Colpitts, "Reduction in the Number of Averages Required in BOTDA Sensors Using Wavelet Denoising Techniques," J. Lightwave Technol. **30**(8), 1134–1142 (2012).
9. X. Qian, X. Jia, Z. Wang, B. Zhang, N. Xue, W. Sun, Q. He, and H. Wu, "Noise level estimation of BOTDA for optimal non-local means denoising," Appl. Opt. **56**(16), 4727–4734 (2017).
10. Y. Muanenda, M. Taki, and F. D. Pasquale, "Long-range accelerated BOTDA sensor using adaptive linear prediction and cyclic coding," Opt. Lett. **39**(18), 5411–5414 (2014).
11. M. A. Soto, J. A. Ramírez, and L. Thévenaz, "Intensifying the response of distributed optical fibre sensors using 2D and 3D image restoration," Nat. Commun. **7**(1), 10870 (2016).
12. Z. Qin, L. Chen, and X. Bao, "Continuous wavelet transform for non-stationary vibration detection with phase-OTDR," Opt. Express **20**(18), 20459–20465 (2012).
13. T. Zhu, X. Xiao, Q. He, and D. Diao, "Enhancement of SNR and spatial resolution in φ-OTDR system by using two-dimensional edge detection method," J. Lightwave Technol. **31**(17), 2851–2856 (2013).
14. F. Wang, W. Zhan, X. Zhang, and Y. Lu, "Improvement of spatial resolution for BOTDR by iterative subdivision method," J. Lightwave Technol. **31**(23), 3663–3667 (2013).
15. G. Soto, J. Fontbona, R. Cortez, and L. Mujica, "An online two-stage adaptive algorithm for strain profile estimation from noisy and abruptly changing BOTDR data and application to underground mines," Measurement **92**, 340–351 (2016).
16. L. Wang, N. Guo, C. Jin, C. Yu, H. Y. Tam, and C. Lu, "BOTDA system using artificial neural network," in Proceedings of 2017 Opto-Electronics and Communications Conference (OECC) and Photonics Global Conference (PGC), (IEEE, 2017).
17. A. K. Azad, F. N. Khan, W. H. Alarashi, N. Guo, A. P. T. Lau, and C. Lu, "Temperature extraction in Brillouin optical time-domain analysis sensors using principal component analysis based pattern recognition," Opt. Express **25**(14), 16534–16549 (2017).
18. M. A. Farahani, E. Castillo-Guerra, and B. G. Colpitts, "Accurate estimation of Brillouin frequency shift in Brillouin optical time domain analysis sensors using cross correlation," Opt. Lett. **36**(21), 4275–4277 (2011).
19. M. A. Farahani, E. Castillo-Guerra, and B. G. Colpitts, "A detailed evaluation of the correlation-based method used for estimation of the Brillouin frequency shift in BOTDA sensors," IEEE Sens. J. **13**(12), 4589–4598 (2013).
20. Y. Mao, N. Guo, K. L. Yu, H. Y. Tam, and C. Lu, "1-cm-spatial-resolution Brillouin optical time-domain analysis based on bright pulse Brillouin gain and complementary code," IEEE Photonics J. **4**(6), 2243–2248 (2012).
21. Y. Dong, H. Zhang, L. Chen, and X. Bao, "2 cm spatial-resolution and 2 km range Brillouin optical fiber sensor using a transient differential pulse pair," Appl. Opt. **51**(9), 1229–1235 (2012).
22. Y. H. Kim, K. Lee, and K. Y. Song, "Brillouin optical correlation domain analysis with more than 1 million effective sensing points based on differential measurement," Opt. Express **23**(26), 33241–33248 (2015).
23. Y. London, Y. Antman, E. Preter, N. Levanon, and A. Zadok, "Brillouin Optical Correlation Domain Analysis Addressing 440 000 Resolution Points," J. Lightwave Technol. **34**(19), 4421–4429 (2016).

Optics EXPRESS

24. A. Denisov, M. A. Soto, and L. Thévenaz, "Going beyond 1000000 resolved points in a Brillouin distributed fiber sensor: theoretical analysis and experimental demonstration," Light Sci. Appl. **5**(5), e16074 (2016).
25. A. Masoudi, M. Belal, and T. P. Newson, "Distributed dynamic large strain optical fiber sensor based on the detection of spontaneous Brillouin scattering," Opt. Lett. **38**(17), 3312–3315 (2013).
26. R. Bernini, A. Minardo, and L. Zeni, "Dynamic strain measurement in optical fibers by stimulated Brillouin scattering," Opt. Lett. **34**(17), 2613–2615 (2009).
27. Y. Peled, A. Motil, L. Yaron, and M. Tur, "Slope-assisted fast distributed sensing in optical fibers with arbitrary Brillouin profile," Opt. Express **19**(21), 19845–19854 (2011).
28. Y. Dang, Z. Zhao, M. Tang, C. Zhao, L. Gan, S. Fu, T. Liu, W. Tong, P. P. Shum, and D. Liu, "Towards large dynamic range and ultrahigh measurement resolution in distributed fiber sensing based on multicore fiber," Opt. Express **25**(17), 20183–20193 (2017).
29. W. Zou, Z. He, and K. Hotate, "Complete discrimination of strain and temperature using Brillouin frequency shift and birefringence in a polarization-maintaining fiber," Opt. Express **17**(3), 1248–1255 (2009).
30. M. A. Soto and L. Thévenaz, "Modeling and evaluating the performance of Brillouin distributed optical fiber sensors," Opt. Express **21**(25), 31347–31366 (2013).
31. M. Nikles, L. Thevenaz, and P. A. Robert, "Brillouin gain spectrum characterization in single-mode optical fibers," J. Lightwave Technol. **15**(10), 1842–1851 (1997).
32. A. Lopez-Gil, M. A. Soto, X. Angulo-Vinuesa, A. Dominguez-Lopez, S. Martin-Lopez, L. Thévenaz, and M. Gonzalez-Herraez, "Evaluation of the accuracy of BOTDA systems based on the phase spectral response," Opt. Express **24**(15), 17200–17214 (2016).
33. L. S. H. Ngia, J. Sjoberg, and M. Viberg, "Adaptive neural nets filter using a recursive levenberg-marquardt search direction," in Proceeding of Conference Record of Thirty-Second Asilomar Conference on Signals, Systems and Computers (Cat. No.98CH36284) (IEEE, 1998), pp. 697–701.